MICRO AND MACRO QUADCOPTER DRONES FOR INDOOR MAPPING TO SUPPORT DISASTER MANAGEMENT

S. Karam [1a, *], F. Nex [1b], O. Karlsson [2a], J. Rydell [2a], E. Bilock [2a], M. Tulldahl [2b], M. Holmberg [2a], N. Kerle [1a]

[1] University of Twente, Faculty ITC, [a]Dept. of Applied Earth Sciences, [b]Dept. of Earth Observation Science, 7514 AE Enschede, The Netherlands
(s.karam, f.nex, n.kerle)@utwente.nl
[2] FOI – Swedish Defence Research Agency, [a]Dept. of Sensor Informatics, [b]Dept. of Electrooptical Systems, P.O. Box 1165, SE-581 11 Linköping, Sweden
(oskar.karlsson, joakim.rydell, erika.bilock, michael.tulldahl, max.holmberg)@ foi.se

Commission I, ICWG I/II

KEY WORDS: Crazyflie, UAV, IMU, micro robot, mobile laser scanning, obstacle avoidance

ABSTRACT:

The use of drones to explore indoor spaces has gained attention and popularity for disaster management and indoor navigation applications. In this paper we present the operations and mapping techniques of two drones that are different in terms of size, the sensors deployed, and the positioning and mapping techniques used. The first drone is a low-cost commercial quadcopter microdrone, a Crazyflie, while the second drone is a relatively expensive research quadcopter macrodrone, called MAX. We investigated their feasibility in mapping areas where satellite positioning is not available, such as indoor spaces. We compared the point clouds obtained by a multi-ranger deck, a multi-layer LIDAR scanner and a stereo camera, and assessed each against ground truth obtained with a terrestrial laser scanner. Results showed that both drones are capable of mapping relatively cluttered indoor environments and can provide point clouds that are sufficient for a quick exploration. Furthermore, the LIDAR scanner-based system can handle a relatively large office environment with an accumulated drift less than 0.02% (1 cm) on the Z-axis and 0.77% (50 cm) on the X and Y axes over a length trajectory of about 65 m. Despite the limited features of the sensor configuration of the Crazyflie, its performance is promising for mapping indoor spaces, given the relatively low deviation from the ground truth: cloud-to-cloud distances measured were generally less than 20 cm.

1. INTRODUCTION

In recent years the scope of indoor mapping has widened to include important applications such as disaster management and indoor navigation. Available indoor mapping systems can be either ground-based or airborne. Some ground-based systems are static, such as terrestrial laser scanners (TLSs); others are trolley-based, such as NavVis[1] M6, hand-held (e.g., GeoSLAM ZEB Revo RT[2]) or backpack-based (Karam et al., 2021). The most popular airborne systems are drones, also called unmanned aerial vehicles (UAVs), which can be either autonomous or semi-autonomous (Dowling et al., 2018).

Drones are commonly used in outdoor applications where they can be autonomous (Colomina et al., 2014), while autonomous flight is more challenging in indoor environments. Therefore, indoor drones are often controlled remotely by an operator. Since drones do not require the operator to access the target area, it is safer to use them in indoor spaces that are inaccessible by the operator due to safety reasons, such as hazardous sites. Because of less space and more obstacles indoors, one of the key challenges of flying drones in indoor spaces is obstacle avoidance. Many drones are equipped with sensors to solve this problem. These work by warning the operator or the autonomous drone of nearby obstacles, preventing the drone from crashing (Lagmay et al., 2019; Greiff, 2017; Raja et al., 2021). In indoor areas global navigation satellite system (GNSS) signals are heavily attenuated or lost; thus, alternative navigational sensors and techniques are required for indoor positioning, such as inertial measurement units (IMUs) and simultaneous localization and mapping (SLAM) algorithms (Wang et al., 2013; Dowling et al., 2018; Aznar et al., 2018). Additionally, UAVs are usually equipped with cameras that can capture indoor environments (Dowling et al., 2018; Wang et al., 2013), while some state-of-the-art systems can also carry light detection and ranging (LIDAR) scanners (Ajay Kumar et al., 2017). While cameras can capture scene texture and they are often used in semantic scene understanding applications (Zhang et al., 2022, 2021), LIDAR can capture the geometry of the building interiors in low-light conditions or in texture-less environments as well (Karam et al., 2019).

In hazardous situations, such as buildings damaged by earthquakes, or situations of fire or toxic gas leaks, drones equipped with such sensors have the capacity to explore unknow indoor environments and to locate victims, making the work of first responders more efficient (Alotaibi et al., 2019; Kulkarni et al., 2020; Paliotta et al., 2021; Tulldahl et al., 2020). While a relatively large drone is needed for high payload capacity, confined or complex indoor environments make the use of these drones impractical. Small-size drones are advantageous to pass through small openings of damaged buildings and provide data for exploration purposes. The generated exploration maps need to quickly deliver the indoor space volumes and shapes to first responders to have a better awareness of the environment and plan swifter and safer rescue activities.

The European Union has funded several research projects focusing on the development of solutions, such as UAVs, for

* Corresponding author

[1] www.navvis.com
[2] www.geoslam.com

disaster management. For example, the Horizon 2020 INGENIOUS project[3], a European and Korean initiative that aims to equip first responders with technologies that can make their jobs safer and more effective. In this paper, we assess the performances of two of the main drones used indoors in this project. The first drone is a low-cost commercial quadcopter microdrone – the Bitcraze Crazyflie 2.1 – and the second is a relatively expensive research quadcopter macrodrone – the Multi-purpose Autonomous eXploring drone (MAX), built by the Swedish Defense Research Agency (FOI) in Linköping, Sweden (Tulldahl et al., 2020). Both drones can be controlled remotely and provide results in real-time. Functions for autonomous MAX operation are being developed. We contrast the performance of both drones for mapping indoor spaces. We also assess the quality of the generated point clouds. This is based on the analysis of three datasets with comparative data, acquired by (i) the Crazyflie and the MAX, (ii) the Crazyflie and a TLS, and (iii) the MAX and a TLS.

The next section of this paper, Section 2, presents a review of related works, while Sections 3 and 4 describe the Crazyflie and MAX drones, respectively. The datasets are explained in Section 5. The experimental results and discussion are presented in Section 6. The paper ends with conclusions in Section 7.

2. RELATED WORK

An increasing number of studies shows the growing role drones can play in search and rescue activities in indoor environments, especially drones that are equipped with one or more sensors (Gao et al., 2019). Various research on indoor mapping with UAVs and LIDAR instruments has been undertaken in the last decade. Cui et al. (2015) integrated visual, LIDAR and inertial sensors in an indoor quadcopter drone. This drone depends on two onboard single-layer Hokuyo LIDAR scanners mounted orthogonally to each other. Their drone weighs 2900 g and has dimensions of 350 mm in height and 860 mm in diagonal width. Therefore, it requires a larger platform and a more powerful motor to fly than the Crazyflie. Using a similar sensor configuration, Ajay Kumar et al. (2017) proposed a LIDAR-based UAV solution for indoor mapping. Fang et al. (2017) customized an aerial vehicle for autonomous navigation through shipboard environments in the event of an emergency. The vehicle was mounted by a depth camera (100 g), an optical flow camera (18 g), a range finder (69 g), a flight controller (38 g) and an embedded computer (70 g). The size of their drone was 580x580x320 mm. Gao et al. (2019) developed a quadcopter UAV equipped with a multi-layer Velodyne scanner (830 g, 103x72 mm) and an IMU for simultaneous localization and mapping.

In contrast to these contributions adopting larger drones, some works used a Crazyflie platform (92x92x29 mm) that has low payload capacity (15 g). For example, Raja et al. (2021) developed a framework for performing localization of a Crazyflie microdrone in the region of flight while simultaneously mapping the region. They used a particle filter-based SLAM algorithm to build a 2D occupancy grid map of an indoor space, using groups of particles as hypothesis of the map generation. To reduce the number of particles, they used LIDAR observations and actuation commands to estimate the pose of the drone. Recent studies on Crazyflie applications used simulated environments, frameworks and platforms (Giernacki et al., 2017; Nithya et al., 2019; Silano et al., 2020; Raja et al., 2021; Duisterhof et al., 2021). Paliotta et al. (2021) utilized multiple microdrones (Crazyflie 2.1) to build a network to localize first responders indoors. These drones require a previously built map of the target area to operate. They are intended to be used with the Loco Positioning System[4], which depends on anchors distributed to estimate the position of the drone in the interior area. The work presented in Giernacki et al. (2017) demonstrated the possibility of determining the 3D position of the Crazyflie drone using a marker attached to its body, a Kinect motion sensing device and a ground station for communication. For collision avoidance, Lagmay et al. (2019) used an infrared sensor to detect obstacles. When an obstacle was detected, their drone was programmed to perform several checks to find an alternative path. However, their framework required a pre-determined model of the area. Duisterhof et al. (2021) used a multi-ranger deck for obstacle detection and avoidance. Some recent works have applied deep learning algorithms to enable a drone to avoid obstacles (Kang et al., 2019; Krishnan et al., 2019). However, these kinds of algorithms require large amounts of data (benchmarks) for training purposes. Having such data is not always possible, and it is difficult to cover all types of indoor environments.

3. MICRODRONE (BITCRAZE CRAZYFLIE 2.1)

Figure 1 shows the microdrone used in this work, a Bitcraze Crazyflie 2.1[5], which is a small (92x92x29 mm), lightweight (27 g), low-cost (281 $) and open source experimental quadcopter released in 2013 by Eliasson et al. (2013). It supports real-time controlling from a ground station with the Crazyradio PA USB radio dongle (about 1 km radio range line-of-sight), and utilizes a small on-board LiPo battery that powers 7 minutes of flight. The Crazyflie is equipped with an IMU sensor and its payload weight is 15 g. For positioning and mapping purposes, we attached a Flow deck V2 and a multi-ranger deck, both sold by Bitcraze, to the Crazyflie drone. Both decks were positioned horizontally and can measure range up to 4 m. The Flow deck was mounted at the bottom of the platform, positioned toward the ground, while the multi-ranger deck was mounted on top of the drone, as shown in Figure 1. Details about the key components of the microdrone are shown in Table 1. The Flow deck provides positioning support. It is composed of two sensors, the VL53L1x time-of-flight (TOF) range finder, which measures the distance to the ground, and the PMW3901 optical flow sensor, a camera that measures movements in relation to the ground. The multi-ranger deck consists of five range finders that provide distance measurements in five different directions with mm precision: front, back, left, right and up.

Components	Weight (g)	Measures range up to	Size (WxHxD) (mm)	Cost ($)
Crazyflie 2.1 (with motors)	27.0	Not applicable	92x92x29	281
Multi-ranger deck	2.3	4 m (5 directions)	35x35x5	112
Flow deck V2	1.6	4 m (one direction)	21x28x4	62

Table 1. The Bitcraze Crazyflie 2.1 microdrone with its key components

[3] https://ingenious-first-responders.eu/

[4] https://www.bitcraze.io/documentation/system/positioning/loco-positioning-system/

[5] https://www.bitcraze.io/products/crazyflie-2-1/

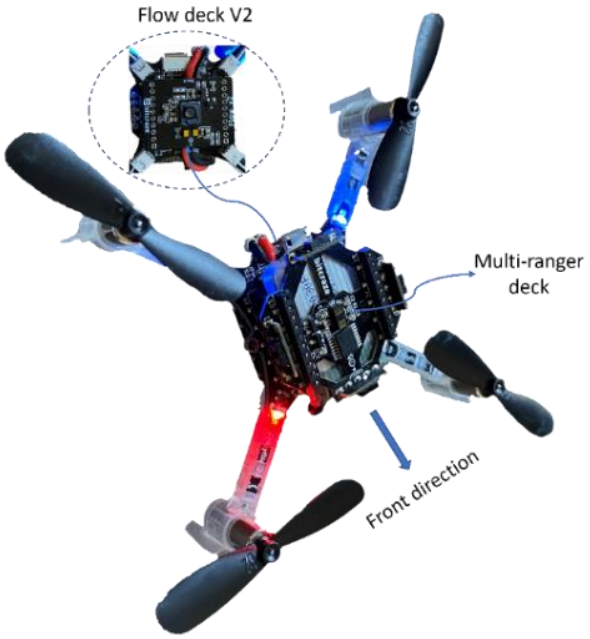

Figure 1. Bitcraze Crazyflie 2.1 drone with attached Flow deck and multi-ranger deck

3.1 Positioning and mapping

For data collection in each test area, the Crazyflie was placed on the floor of the test area, pointing away from the controller (the computer keyboard) to facilitate the control task. We used the Crazyflie python library (cflib)[6], an open-source application programming interface, to easily control and communicate with the Crazyflie. The Crazyflie first takes off and hovers at a height of 30 cm.

The pose of the Crazyflie is estimated using an extended Kalman filter (EKF)-based state estimator developed by Bitcraze, based on Greiff (2017) and Mueller et al. (2017). This estimator utilizes the IMU observations of angular velocities and accelerations, in cooperation with the Flow deck, to estimate the state of the Crazyflie. Specifically, the observations of the TOF sensor in the Flow deck are exploited to estimate the translation along the Z-axis, while the optical flow sensor captures the movements in the XY plane based on visual feature matching.

As the purpose is mapping the indoor environments, we recorded the laser points measured by the multi-ranger deck and the Flow deck TOF sensor. The ground station displayed the recorded points over time. This enabled observation of the mapping process during flight. To cover the target area, we used a keyboard to remotely control and update the Crazyflie state. For example, we could rotate it around its vertical axis, or move it forward, backward, right and left. This was implemented through changing the linear or rotational velocity of the Crazyflie along the target direction by a specific factor. This change in the velocity was used for updating the pose parameters.

The origin of the local coordinate system was assumed to be at the start point. At the end of data collection, the recorded points formed a point cloud described in this local system (see Figure 7). The presented position and mapping system does not perform loop closure that can enable the drone to recognize a previously visited space and correct the drift.

[6] https://github.com/bitcraze/crazyflie-lib-python

3.2 Obstacle avoidance

The implemented obstacle avoidance technique does not need any external positioning system or additional sensor. The Crazyflie, using the Flow deck and multi-ranger deck, can measure distance in all directions and avoids any object within 20 cm by applying a movement velocity along the opposite direction of the detected obstacle. The Crazyflie prevents movement in the direction of the obstacle, even if the operator sends a command to move in that direction. Instead, the Crazyflie sends the operator a warning message alerting them to the existing obstacle. Based on this alert and the up-to-date visualization map on the screen, the operator must search for an alternative path. As the goal of this study is to evaluate the use of the drone in indoor spaces, which sometimes are inaccessible, this avoidance technique enables the Crazyflie to avoid obstacles, even if the operator does not have a clear line of sight with the drone.

4. MAX DRONE

Figure 2 shows the MAX drone and the components used for on-board positioning and mapping. It is a realisation of the system described in Tulldahl et al. (2020). The drone is currently under development within the INGENIOUS project. The MAX drone is a custom platform built to accommodate two independent positioning systems; the LIDAR-based system described in Section 4.1, and the camera-based system described in Section 4.2. Both systems generate a 3D point cloud of the mapped environment. The configuration consists of a LIDAR with a 100 m range (Ouster OS1-16), tilted and mounted on the top of the platform; a stereo camera with a 10 m range (Intel RealSense D435i); and a controller (3DR Pixhawk Mini) managed by a Raspberry Pi 4 Model B. Details about the main positioning components are shown in Table 2, where the size and weight of the entire drone (2700 g) includes computing modules, cables, etc. The Ouster scanner weighs 400 g and costs 3,500 $, while the stereo camera weighs 72 g and costs 320 $. The flight time for this setup is around 4 minutes.

The MAX drone is intended to be used by first responders, to fly autonomously into buildings and send multi-sensor data back to a ground control station.

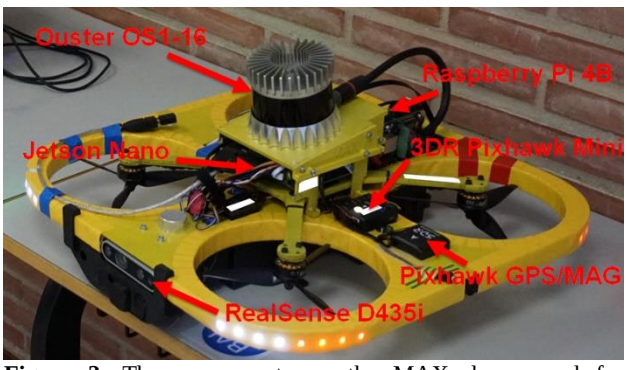

Figure 2. The components on the MAX drone used for positioning and mapping.

4.1 LIDAR-based Grape system

The LIDAR based positioning system on-board the MAX drone, GRAph-based Precision lasEr (Grape), was first presented in Tulldahl et al. (2020). The system runs in real time on the

Component	Weight (g)	Maximum range (m)	Size (WxHxD) (mm)	Cost ($)
MAX drone (with battery)	2700	Not applicable	420x210x430	Not applicable
Ouster OS1-16 LIDAR	400	100	83x73x83 (cylinder)	3,500
RealSense D435i	72	10	90x25x25	320

Table 2. The main components of the MAX drone.

Raspberry Pi 4B using the robot operating system (ROS[7]) and Georgia Tech Smoothing and Mapping (GTSAM[8]) frameworks. The Ouster LIDAR has a 360° horizontal and 33.2° vertical field of view. It operates at a 10 Hz scanning frequency and records about 330,000 laser points per second. Features in the form of planes and edges are extracted from each LIDAR scan (Zhang and Singh, 2014). These features are then associated with the up-to-date built map and fed into the graph-based SLAM algorithm incremental smoothing and mapping (iSAM2) (Kaess et al., 2012), together with accelerometer and gyroscope data from the built-in IMU in the Pixhawk. Loop closure was not yet implemented which results in a reduced accuracy over longer time periods. A more detailed explanation of the system can be found in Tulldahl et al. (2020). The resulting 3D point cloud from the Grape system (MAX Grape cloud) is generated by transforming the LIDAR data into estimated position. This is completed onboard at 1 Hz because of the rate used by the high-level planning algorithm.

4.2 Camera-based Kiwi system

The Kiwi system uses a stereo camera and an IMU for positioning and mapping. The position is computed using an EKF SLAM algorithm (Rydell and Bilock, 2015), which is popular in real-time navigation applications (Lin et al., 2021). The algorithm is based on tracking visual landmarks in consecutive images. The IMU aids the landmark tracking, while the accelerometer and gyroscope data are used to predict where landmarks are expected to appear in an image. It also provides positioning, although with reduced precision, during brief passages through dark or featureless environments. The Kiwi is based on previously published work on a series of positioning systems known as the Chameleon (Rydell and Bilock, 2012; 2015). Its theoretical background is presented in more detail in Veth et al. (2007).

Since the system does not recognize previously visited locations, the estimated position drifts over time (the error is typically about 1% of the travelled distance). This can be corrected using methods for loop closure, but this was not yet implemented in the real-time system in this test.

A map is created by merging transformed local point clouds from the depth-sensing stereo camera. Each point cloud is transformed according to the estimated position and orientation of the camera at the time the point cloud was acquired. Hence, the map is represented as a set of points (MAX Kiwi cloud).

The algorithms run in real-time on an Nvidia Jetson Nano embedded computer onboard the MAX drone. The RealSense stereo camera used by the system provides high-quality images in terms of geometric calibration and image noise, and uses a global shutter. The built-in IMU in this camera, however, is relatively simple, which limits the achievable performance in environments where landmarks are not always available. The horizontal field of view of the camera is approximately 90°.

5. TEST AREAS

Three datasets were used in this work. The first dataset, named Berrozi, was collected in one of the technical-tactical training facilities for the Basque police force (Ertzaintza) in Berrozi, Spain. Both Crazyflie and MAX drones mapped an indoor space in this facility. The mapped area was a room that contained a wooden wall and pillar of carton boxes in the middle, as well as several tables and chairs, resulting in a relatively cluttered indoor environment (Figure 3). These characteristics made the room a suitable area to rigorously test the capability of the presented drones and the employed obstacle avoidance technique in the Crazyflie. Additionally, this dataset was used to compare the performance of both drones.

For the second dataset, named ITC, we scanned an area in the emergency exit staircase in the University of Twente, Faculty of Geo-Information Science and Earth Observation (ITC) building in Enschede, the Netherlands, with the Crazyflie. It is an environment with a variance in the height to the ceiling. This dataset was used to evaluate the performance of the Crazyflie in mapping indoor spaces, against ground truth obtained by a TLS for the same area. We used RIEGL TLS that provides scan data acquisition with 5 mm accuracy.

The third dataset was captured indoors with the MAX drone in a larger office environment at FOI. This was also compared to a TLS used for ground truth of the area. The room consists of some concrete pillars, various furniture and equipment and is about 25 m at the widest. For this dataset, a FARO TLS with an accuracy of less than 5 mm was used. This TLS provides color data for each 3D point.

6. EXPERIMENTAL RESULTS AND DISCUSSION

In this section, we first compare the obtained point clouds from both drones. Next, we present the results of each drone against ground truth data obtained by a TLS. The point clouds include some outlying points that were captured through glass. As these points will often not be present in both clouds, we excluded them from the comparison.

6.1 Crazyflie & MAX comparison

As both Crazyflie and MAX drones consider the start point to be the origin of the model coordinate system, each drone started at the same point on the floor. The Crazyflie was flown manually, while the MAX drone was carried around the room. Each drone scanned the room in Berrozi, and the generated cloud from the Crazyflie (Figure 4) was compared to the MAX Kiwi cloud (Figure 3) and the MAX Grape cloud (Figure 5).

As the range finders on the Crazyflie perform 2D scanning, they do not generate 3D point clouds as do the 3D LIDAR and camera-based systems onboard the MAX drone. Instead, the Crazyflie provides a 2D point cloud map consisting of points captured on the surrounding walls using the side range finders (Figure 4). Additionally, it provides points on the ceiling and floor, which

[7] https://www.ros.org/

[8] https://gtsam.org/

correspond to the followed trajectory, using the vertical range finders (Figure 7).

For comparison purposes we segmented out MAX Kiwi points that corresponded to Crazyflie cloud in terms of the flight altitude. However, when we plotted clouds from both drones together, they were not precisely aligned with the same coordinate system, since they did not start in the same orientation. Therefore, we registered both clouds in the same coordinate system by means of coarse registration and the iterative closest point (ICP) algorithm included in the open-source free CloudCompare software. To quantify the deviation of Crazyflie cloud from the MAX Kiwi cloud, we computed the cloud-to-cloud absolute distances (Figure 4). MAX Kiwi generated the point cloud using the SLAM algorithm presented in Section 4.2, while the Crazyflie uses the Flow deck and multi-ranger deck ($\leq$ 4 m) for mapping. Results showed that the Crazyflie performance is comparable to the MAX drone, as about 87% of the cloud-to-cloud distances between the corresponding clouds from both drones were within a range of less than 20 cm.

However, Figure 3 shows sparse points on three different sides of the MAX Kiwi cloud, compared to almost linear points in the Crazyflie cloud (Figure 4). The main reason behind this discrepancy is related to the different sensor configuration and the flight height during mapping. Specifically, MAX was operating on a flight level ($>$ 1 m) higher than the surfaces of the tables and chairs that were located near the walls in these three sides, while the Crazyflie flew at a height of 30 cm from the floor. Therefore, the wall, which was clearly visible for the Crazyflie, was heavily occluded by the tables and chairs for the MAX. The registered 3D point cloud and trajectory from the LIDAR-based Grape system onboard the MAX drone can be seen in Figure 5. The cloud was cleaned from clutter and compared to the Crazyflie point cloud. The cloud-to-cloud distances shown in Figure 6 demonstrate that over 96% of the distances were in a range of less than 20 cm.

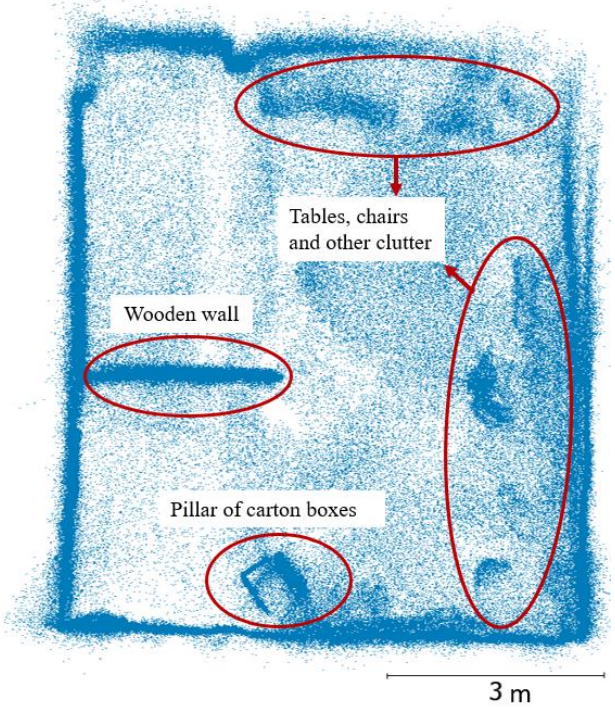

Figure 3. Top view of the MAX Kiwi map (3D point cloud) for the Berrozi dataset.

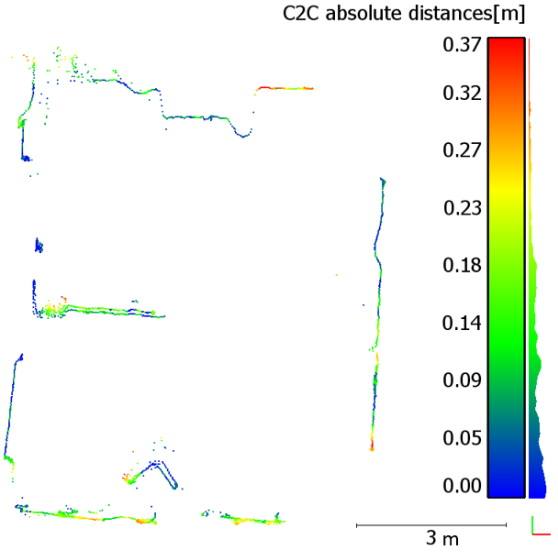

Figure 4. Crazyflie point cloud map, coloured based on point distance to the MAX Kiwi map, in the Berrozi dataset.

When this dataset was collected, the drone moved along a closed loop, such that the start and end positions were identical. Since the Grape system did not perform loop closure correction at the end of the loop, it accumulated a drift of about 1.07% (15 cm) on the X and Y axes, and 0.07% (1 cm) in the Z-axis direction over a length trajectory of about 13-14 m. The significant drift introduced duplicate walls into the generated point cloud as shown in Figure 5.

When repeating the experiment for a more reliable comparison of the drones, a clearly marked location and direction for each drone take-off should be used to reduce user error, and to ensure that the coordinate systems of comparison flights are aligned. Additionally, both drones should hover at the same height.

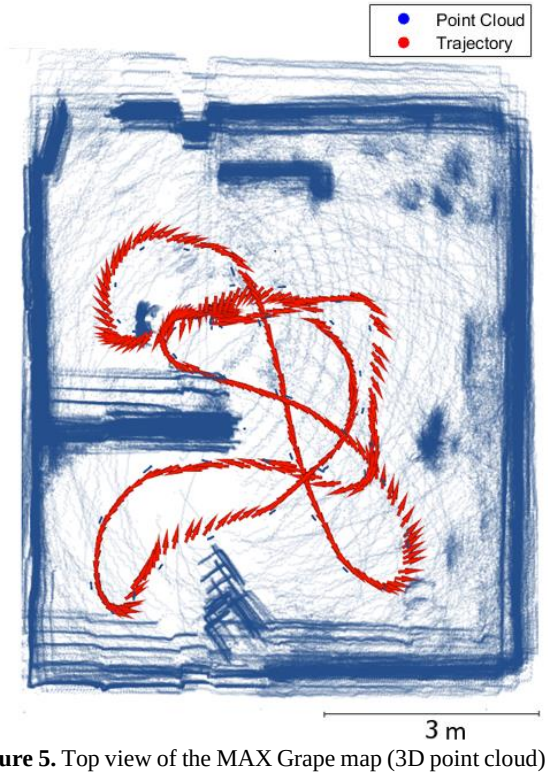

Figure 5. Top view of the MAX Grape map (3D point cloud) and trajectory in the Berrozi dataset.

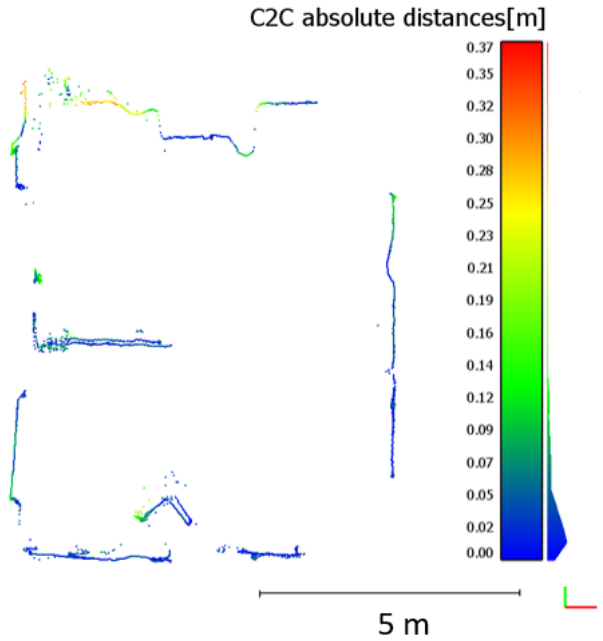

Figure 6. Crazyflie point cloud map, coloured based on point distance to the MAX Grape map, in the Berrozi dataset.

6.2 Crazyflie & TLS comparison

To verify the internal quality and consistency of the Crazyflie point cloud, it was compared to a TLS map, which is considered to be internally properly aligned. First, we computed the deviation of the Crazyflie map to the TLS map used as ground truth (Figure 9). Second, we extracted geometric distance information (Figure 7) from each map for comparison purposes (Table 3).

Similar to the previous comparison, the 2D point cloud map derived from the Crazyflie and the corresponding map from the TLS (Figure 8) were registered on the same coordinate system. Figure 9 shows that about 93% of the cloud-to-cloud distances were less than 20 cm.

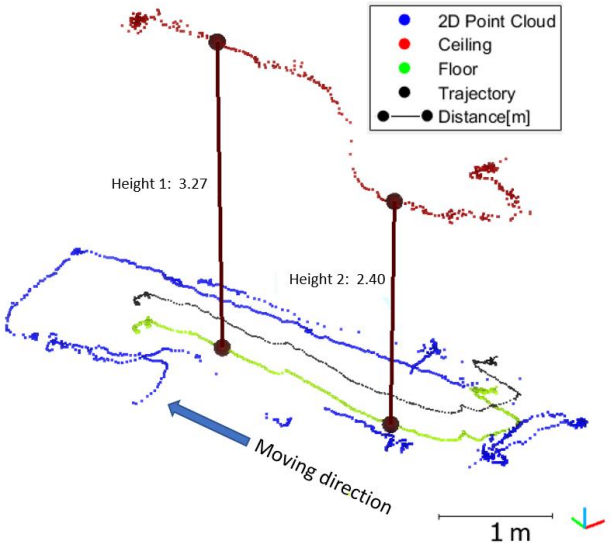

Figure 7. Slanted view of the Crazyflie 2D point cloud map with trajectory, ceiling and floor points and some height measurements for the ITC dataset

The largest deviation was seen in the direction of movement, as points on the surfaces behind and in front of the Crazyflie had the highest cloud-to-cloud distances. This happened because the Crazyflie sometimes did not capture any motion and glided away because it was flying over a visually featureless floor. This also explains why the drone drifted at the end of the trajectory while turning around, which in turn led to double lines of points on the walls to the right and left of the moving direction (Figure 7).

Since the vertical range finders on the Crazyflie support the estimation of translation along the Z-axis, the drift along this axis direction was smaller than the drift along other axes. This was evident through its ability to capture the change in the ceiling height with cm precision, as shown in Figure 7 and Table 3.

Height	Crazyflie (m)	TLS (m)
Height 1	3.27	3.29
Height 2	2.40	2.41

Table 3. Distances between the floor and the ceiling from the TLS and Crazyflie point cloud maps

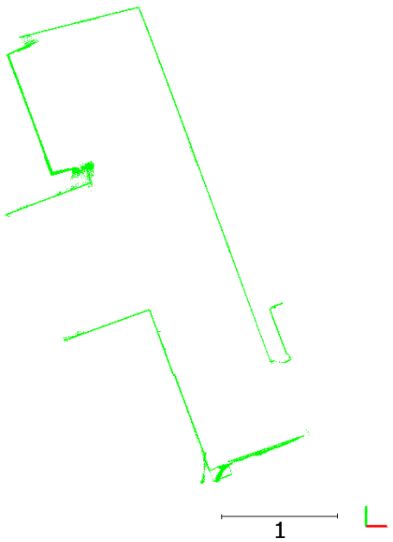

Figure 8. 2D point cloud, segmented out of the TLS point cloud at Crazyflie scanning height, for the ITC dataset

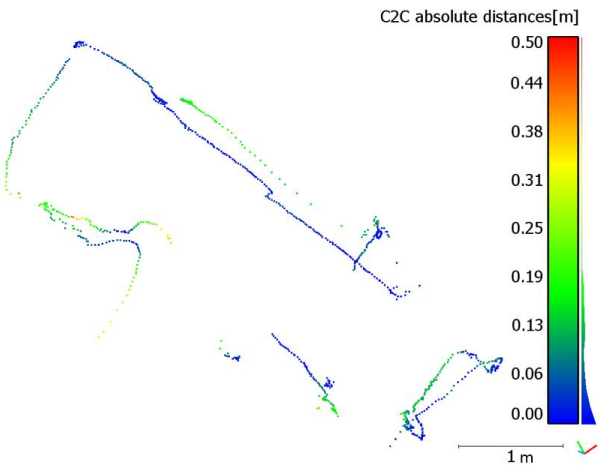

Figure 9. Crazyflie 2D point cloud map, coloured based on point distance to the TLS map, for the ITC dataset.

6.3 MAX and TLS comparison

To generate the third dataset, an office environment at FOI was captured by the MAX drone and a TLS. Also in this experiment, MAX was carried during data acquisition. Figure 10 shows the generated point clouds using the LIDAR-based Grape system and the TLS. The results of cloud-to-cloud matching showed that 75% of the distances were below 20 cm (Figure 10), and the deviation between the start and end positions was below 0.02% (1 cm) in the Z-axis direction and less than 0.77% (50 cm) on the X and Y axes for a travelled distance of about 65 m.

The TLS visualization and the corresponding point cloud from the camera-based Kiwi system can be seen in Figure 11. Matching these point clouds showed that 80% of the distances were below 30 cm, and 55% of the distances were less than 20 cm. The start-end error of the trajectory was approximately 0.5 m in both the horizontal and vertical directions. It should be noted that most of the furniture in the room was moved between the TLS and the Kiwi measurements. This may cause an overestimation of the point distances. Positioning from the Grape and Kiwi systems are fused onboard, a process that is not covered in this paper. Ongoing work on loop closure for both systems will improve performance in areas of current difficulties.

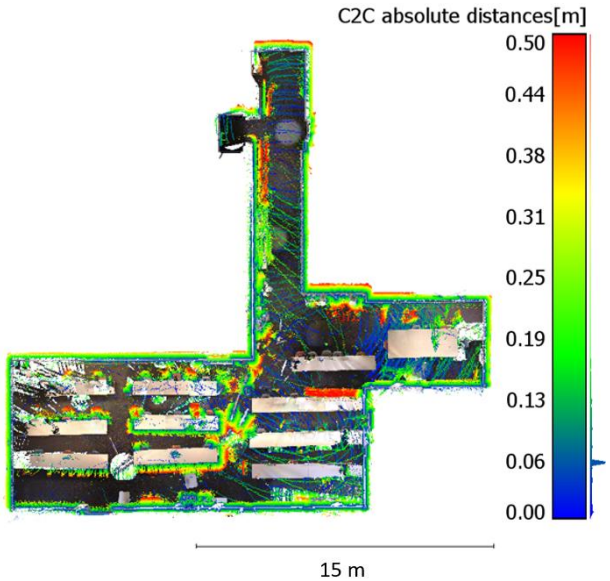

Figure 10. Top view of the TLS point cloud map (the ceiling points are not shown in order to show the interior structure) and Grape point cloud (coloured based on point distance to the TLS map) for the FOI dataset.

7. CONCLUSIONS AND FUTURE WORK

This paper presents two drones, Crazyflie and MAX, with different configurations and capabilities. Experimental results show that both drones are capable of mapping indoor environments and can provide point clouds that are sufficient for exploration purposes.

Although the Crazyflie has limited sensor abilities, it showed promising performance in mapping small indoor spaces. This is evident from the relatively low deviation of its point cloud in comparison to the MAX drone, and the TLS measurements that served as truth. In future work, we intend to integrate complementary sensors, such as a thermal camera, to increase the efficiency of the Crazyflie. Additionally, we will fly the drone at different heights to provide better coverage of the mapped space.

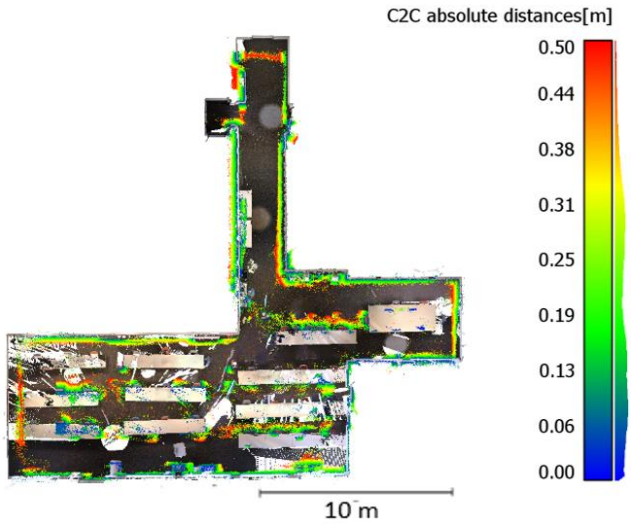

Figure 11. Top view of the TLS point cloud map (the ceiling points are not shown in order to show the interior structure) and Kiwi point cloud (coloured based on point distance to the TLS map) for the FOI dataset.

The LIDAR-based Grape system onboard the MAX drone did not perform well in the smaller Berrozi environment, but showed improved results in larger environments, such as the FOI office environment, where it benefits from its range and 360° view. The camera-based Kiwi system worked very well in the smaller Berrozi environments, but showed slightly larger errors in the larger FOI environment. As of now, the MAX drone does not have obstacle avoidance capability, but this is to be implemented in the near future.

ACKNOWLEDGEMENTS

The INGENIOUS project has received funding from the European Union's Horizon 2020 Research and Innovation Programme and the Korean Government under Grant Agreement No 833435. Content reflects only the authors' view and the Research Executive Agency (REA) and the European Commission are not responsible for any use that may be made of the information it contains. The authors would like to thank Mr. Kristoffer Richardsson from the Bitcraze team for the exchange of correspondence.

REFERENCES

Ajay Kumar, G., Patil, A.K., Patil, R., Park, S.S., Chai, Y.H., 2017. A LiDAR and IMU integrated indoor navigation system for UAVs and its application in real-time pipeline classification. *Sensors* 17, 1268. https://doi.org/10.3390/s17061268

Alotaibi, E.T., Alqefari, S.S., Koubaa, A., 2019. LSAR: multi-UAV collaboration for search and rescue missions. *IEEE*, 55817–55832. https://doi.org/10.1109/ACCESS.2019.2912306

Aznar, F., Pujol, M., Rizo, R., Pujol, F.A., Rizo, C., 2018. Energy- efficient swarm behavior for indoor UAV ad-hoc network deployment. *Symmetry (Basel)*. 10, 1–15. https://doi.org/10.3390/sym10110632

Blaser, S., Nebiker, S., Wisler, D., 2019. Portable image-based high performance mobile mapping system in underground environments - system configuration and performance evaluation. *ISPRS Ann. Photogramm. Remote Sens. Spat. Inf. Sci.* 4, 255–262. https://doi.org/10.5194/isprs-annals-IV-2-W5-255-2019

Bouabdallah, S., Siegwart, R., 2007. Full control of a quadrotor. *IEEE Int. Conf. Intell. Robot. Syst.* 153–158. https://doi.org/10.1109/IROS.2007.4399042

Colomina, I., Molina, P., 2014. Unmanned aerial systems for photogrammetry and remote sensing: A review. *ISPRS J. Photogramm. Remote Sens.* 92, 79–97. https://doi.org/10.1016/j.isprsjprs.2014.02.013

Cui, J.Q., Phang, S.K., Ang, K.Z.Y., Wang, F., Dong, X., Ke, Y., Lai, S., Li, K., Li, X., Lin, F., Lin, J., Liu, P., Pang, T., Wang, B., Wang, K., Yang, Z., Chen, B.M., 2015. Drones for cooperative search and rescue in post-disaster situation. Proc. 7th IEEE Int. Conf. Cybern. Intell. Syst. CIS Robot. Autom. Mechatronics, RAM 167–174. https://doi.org/10.1109/ICCIS.2015.7274615

Dowling, L., Poblete, T., Hook, I., Tang, H., Tan, Y., Glenn, W., Unnithan, R.R., 2018. Accurate indoor mapping using an autonomous unmanned aerial vehicle (UAV). [online], Available: https://arxiv.org/abs/1808.01940 (accessed Dec. 2021).

Duisterhof, B.P., Krishnan, S., Cruz, J.J., Banbury, C.R., Fu, W., Faust, A., de Croon, G.C.H.E., Janapa Reddi, V., 2021. Tiny Robot Learning (tinyRL) for Source Seeking on a Nano Quadcopter. *IEEE International Conference on Robotics and Automation (ICRA)*, 7242–7248. https://doi.org/10.1109/icra48506.2021.9561590

Fang, Z., Yang, S., Jain, S., Dubey, G., Roth, S., Maeta, S., Nuske, S., Zhang, Y., Scherer, S., 2017. Robust autonomous flight in constrained and visually degraded shipboard environments. *J. F. Robot.* 34, 25–52. https://doi.org/10.1002/rob.21670

Gao, F., Wu, W., Gao, W., Shen, S., 2019. Flying on point clouds: Online trajectory generation and autonomous navigation for quadrotors in cluttered environments. *J. F. Robot*. 36, 710–733. https://doi.org/10.1002/rob.21842

Giernacki, W., Skwierczy, M., Witwicki, W., Kozierski, P., 2017. Crazyflie 2.0 quadrotor as a platform for research and education in robotics and control engineering. *IEEE*. 37–42.

Greiff, M., 2017. Modelling and control of the crazyflie quadrotor for aggressive and autonomous flight by optical flow driven state estimation. M.S. thesis, Dept. of Automatic Control, Lund University, Sweden. 153.

Kaess, M., Johannsson, H., Roberts, R., Ila, V., Leonard, J.J., Dellaert, F., 2012. ISAM2: Incremental smoothing and mapping using the Bayes tree. *Int. J. Rob. Res.* 31, 216–235. https://doi.org/10.1177/0278364911430419

Kang, K., Belkhale, S., Kahn, G., Abbeel, P., Levine, S., 2019. Generalization through simulation: Integrating simulated and real data into deep reinforcement learning for vision-based autonomous flight. *Proc. - IEEE Int. Conf. Robot. Autom.* 2019-May, 6008–6014. https://doi.org/10.1109/ICRA.2019.8793735

Karam, S., Lehtola, V., Vosselman, G., 2021. Simple loop closing for continuous 6DOF LIDAR&IMU graph SLAM with planar features for indoor environments. *ISPRS J. Photogramm. Remote Sens.* 181, 413–426. https://doi.org/10.1016/j.isprsjprs.2021.09.020

Karam, S., Vosselman, G., Peter, M., Hosseinyalamdary, S., Lehtola, V., 2019. Design, calibration, and evaluation of a backpack indoor mobile mapping system. *Remote Sens*. 11. https://doi.org/10.3390/rs11080978

Krishnan, S., Boroujerdian, B., Fu, W., Faust, A., Reddi, V.J., 2019. Air learning: an AI research platform for algorithm-hardware benchmarking of autonomous aerial robots. CoRR, vol. abs/1906.00421, 2019. [Online]. Available: http://arxiv.org/abs/1906.00421 .

Kulkarni, S., Chaphekar, V., Chowdhury, M.M.U., Erden, F., Guvenc, I., 2020. UAV aided search and rescue operation using reinforcement learning. *Conf. Proc. - IEEE SOUTHEASTCON* 2. https://doi.org/10.1109/SoutheastCon44009.2020.9368285

Lagmay, J.M.S., Jed Leyba, L.C., Santiago, A.T., Tumabotabo, L.B., Limjoco, W.J.R., Michael Tiglao, N.C., 2019. Automated indoor drone flight with collision prevention. *IEEE Reg. 10 Annu. Int. Conf. Proceedings/TENCON*, 1762–1767.https://doi.org/10.1109/TENCON.2018.8650371

Lin, J., Zheng, C., Xu, W., Zhang, F., 2021. R2LIVE: A robust, real-time, LiDAR-inertial-visual tightly-coupled state estimator and mapping. . *IEEE Robot. Autom. Lett*, 6, 7469–7476

Eliasson, M., Taffanel, A., Antonsson, T., 2013. Tiny, hackable quadcopter drone launches pre-orders. *WIRED*. URL https://www.wired.com/2013/02/crazyflie-nano/ (accessed Dec. 2021).

Mueller, M.W., Hehn, M., D'Andrea, R., 2017. Covariance correction step for Kalman filtering with an attitude. J. Guid. Control. Dyn. 40, 2301–2306. https://doi.org/10.2514/1.G000848

Nithya, M., Rashmi, M.R., 2019. Gazebo - ROS - simulink framework for hover control and trajectory tracking of Crazyflie 2.0. *IEEE Reg. 10 Annu. Int. Conf. Proceedings/TENCON*, 649–653. https://doi.org/10.1109/TENCON.2019.8929730

Paliotta, C., Ening, K., Albrektsen, S.M., 2021. Micro indoor-drones (MINs) for localization of first responders. *In Proceedings of the 18th ISCRAM*, Blacksburg, VA, USA.

Raja, G., Suresh, S., Anbalagan, S., Ganapathisubramaniyan, A., Kumar, N., 2021. PFIN: an efficient particle filter-based indoor navigation framework for UAVs. *IEEE Trans. Veh. Technol.* 70, 4984–4992. https://doi.org/10.1109/TVT.2021.3072727

Rydell, J., Bilock, E., 2015. Panther chameleon: real-time image-based positioning and mapping. *Inst. Navig. Int. Tech. Meet.* 768–777.

Rydell, J., Emilsson, E., 2012. Chameleon: Visual-inertial indoor navigation. *IEEE/ION Position, Locat. Navig. Symp.* 541–546.

Silano, G., Iannelli, L., 2020. CrazyS: a software-in-the-loop simulation platform for the Crazyflie 2.0 nano-quadcopter. in *Robot Operating System (ROS), The Complete Reference*, vol. 4, A. Koubaa, Ed. Springer https://doi.org/10.1007/978-3-030-20190-6_4

Tulldahl, M., Holmberg, M., Karlsson, O., Rydell, J., Bilock, E., Axelsson, L., Tolt, G., Svedin, J.A., 2020. Laser sensing from small UAVs. *Electro-Optical Remote Sens. XIV. Int. Soc. Opt. Photonics.* https://doi.org/10.1117/12.2575933

Wang, F., Cui, J.-Q., Chen, B.-M., Lee, T.H., 2013. A comprehensive UAV indoor navigation system based on vision optical flow and laser FastSLAM. *Acta Autom. Sin.* 39, 1889–1899. https://doi.org/10.1016/s18741029(13)60

Zhang, J., Singh, S., 2014. LOAM : lidar odometry and mapping in real - time. in *Robotics: Science and Systems*, vol. 2, no. 9, https://doi.org/10.15607/RSS.2014.X.007

Zhang, N., Nex, F., Kerle, N., Vosselman, G., 2022. LISU: Low-light indoor scene understanding with joint learning of reflectance restoration. *ISPRS J. Photogramm. Remote Sens.* 183, 470–481. https://doi.org/10.1016/j.isprsjprs.2021.11.010

Zhang, N., Nex, F., Kerle, N., Vosselman, G., 2021. Towards learning low-light indoor semantic segmentation with illumination-invariant features. *Int. Arch. Photogramm. Remote Sens. Spat. Inf. Sci. - ISPRS Arch.* 43, 427–432. https://doi.org/10.5194/isprs-archives-XLIII-B2-2021